

Direct Normal Irradiance Prediction By Using Cloud Tracking Method

Chih-Chieh Ma, I-Tao Lung
Instrumentation Division
Institute of Nuclear Energy Research

Abstract

The accumulated installed PV capacity around the world was 233 GW at the end of 2015, and is projected to reach 1000 GW in 2026. However, the intermittent nature of solar energy might cause a problem with high solar penetration. To elude the problem, an accurate solar energy forecast is needed. There are many ways to do the short-term solar forecasting such as the statistical methods, e.g., artificial neural networks and linear regression, but in those methods the physical quantities are not taken into account. In this study, digital sky images acquired by Yankee's Total Sky Imager (TSI-880) [1] are processed in pixel-wise and classified into clear sky, optically thick and optically thin clouds to provide cloud cover information. Furthermore, a scheme was provided to identify the cloud movement in conditions of no significant changes in cloud geometry. To carry on the calculation and assessment of the cloud group movement by comparing two consecutive cloud images, authors detect the velocity of the cloud group vector, and make an extrapolation to project the future cloud position to see if the cloud blocks the sun, making the Direct Normal Irradiance (DNI) decayed. By computing the cloud shadowing factor, thus DNI forecasting can be fulfilled.

Key word: Total Sky Imager, Direct Normal Irradiance, forecast

1. Introduction

In general, the international studies on the sky image processing take the following steps: (1) defining contours range, removing the shadow-band and imager support arm: a study reported by Jiunn-Lin Wu [2], et al. conducts it by using image inpainting to remove dust spots from digital-SLR images; (2) restoring distortion image: Ricardo Marquez [3] completes it in intra-hour DNI forecasting based on cloud tracking image analysis; (3) interpreting and computing sky image: in 2014, Zhu Xiang [4] et al. implement it in all-sky cloud map image restoration algorithm research and Ding Yuyu [5] et al. fulfill it in the forecasting of global horizontal irradiance in photovoltaic power stations based on the total sky imager. Among all the studies mentioned above, there is no paper elaborating the integrated step to compute the cloud cover. In this study, authors utilize the images of September 11 of 2014 at Longtan, Taiwan, to demonstrate the entire process of handling the cloud cover image.

2. Cloud Image Repairing and Restoration Defining Contours Range

From the point of view of the original output images, TSI-880 reflects the sky hemisphere, but also reveals the fuselage structure of the equipment. Through further scrutinizing, the metal hemispherical reflected sky image more or less includes the nearby landscape such as trees, facilities or buildings around the installation site. The spherical body part and the rim of

TSI-880 actually make less influence on the observation of cloud and irradiance, so they can be neglected.

Seeking the Pixel Center

The practical test shows that the pixel center of the original output image of TSI-880 is not the de facto hemisphere rotation center because the shadow belt and camera support, buildings and trees in the image are to be removed by a series of image process. If the rotation center is set off, the subsequent creation of the automatic shadow belt mask of image repairing will be unable to match the actual position of the shadow belt, resulting in the image repairing incomplete, i.e., the shadow belt cannot be removed completely. Therefore, it needs to oftentimes confirm the automatically generated mask is matching with the one of the sky imager and the relevant verification procedure is described in the section of Automatic Mask Generation.

Image Selection Determination

After the pixel center is found, the cloud radius will be gradually reduced by decreasing its percentage in order to observe whether the unwanted near-surface objects are fully removed. The TSI-880 installed at INER is on the roof with no particular tall objects around; therefore, the ratio of 85% of the original radius is reasonably taken to remove all the surplus objects within the range of 360 degrees, which spares the extra repairing step of deleting the objects. The scope of the original cloud and selected cloud are shown in Figure 1

and Figure 2.



Fig.1 Original Cloud Image Fig.2 Selected Cloud Image

Removing the Shadow-band and Imager Support Arm

To avoid long-term exposure to the sun, causing aging or failure of sky imager camera sensing elements, there is a light shielding tape sticks to the metal hemispherical surface, forming the shadow belt in the imagery, while the metal hemispherical surface rotates, the tape moves around accordingly. However, it not only covered the sun, but also obscured the sky region from the center to the fringe of the entire strip portion. In addition, the camera is fixed to the brim of the bracket, causing the reflection on the surface, also shelters a small part of the sky. The aggregate proportion of those two partially obscured sky occupied by about 8 to 9 percent of the image, bringing about a certain degree of error in the calculation of cloud amount. With the image processing of the inpainting technology, those shaded parts can be reasonably restored, which improves the accuracy of estimating the quantity of cloud.

Automatic Mask Generation

In the image patch implementation, the first step required is to build the mask, which should be consistent with the original size of the objects. The mask is usually in black and white, while the black represents the original image region should be kept, the white area represents the object is to be removed, of which as previously described are the shadow belt and the camera support. To duplicate the feature of the shadow belt, an automatic calculation method must be developed to calculate the position of the sun at every time frame, and then draws the mask from the center to the edge of the surface. Figure 3 shows the automatically generated mask at different time of August 15, 2014.



Fig.3 Automatically Generated Mask

Cloud Image Inpainting

To test the effect of different imaging patch repairing (aka inpainting) algorithms on cloud, three

different algorithms are implemented, i.e., local binary pattern based texture inpainting, Navier-Stokes based method and the fast marching method of Alexandru Telea, shown as in figure 4. The first one utilizes the conjecture of material synthesis, while the latter two make use of the partial differential equations. From the analysis results, the repaired sky cloud image of the material synthesis method is apparently incompatible with the original imagery surroundings due to the sky cloud is not uniform, which is not suitable for the material synthesis method. As a result, the inpainting performance on the rest two kinds of partial differential equations renders little difference. After removing the shadow belt, there was a clear ambiguity phenomenon around the removed area partly because of the diffusion effect, partly because of wider strip belt. For the camera bracket part, the diffusion phenomenon is not obvious for the removed area is slender. Making a careful comparison of the two repairing effect of the partial differential equation, the blurring effect of the Fast Marching Method is less than the one of Alexandru Telea.

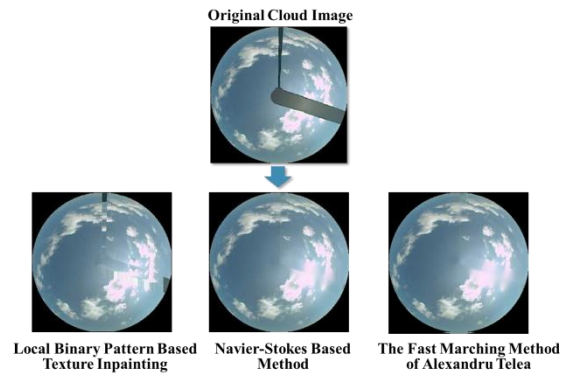


Fig.4 Different Algorithms of Inpainting

Image Distortion Restoration

Compared to the flat surface mode, the sky cover area reflected by the metal hemisphere is much larger, about 10 km in radius. However, the image is distorted owing to curved surface taken. At the center portion is enlarged, and the edge portion of the image is compressed, resulting in a considerable amount of error when calculating the cloud. Therefore, the image distortion restoration is needed to get the correct image cloud.

Radial Distortion Recovery

To restore the curved surface sky image, the following information is required: the dimension of the hemispherical metal camera bracket, the camera position and geometric location data, as well as the focal length of the camera lens and other optical materials. In the report of Ricardo Marquez, a method based on the relationship between cloud time and solar zenith angle is described. It mainly deals with restoring the curved image. In a polar

coordinates view, the distortion is in the radial direction outward from the center to the brim. Each dot pixel of the curved surface from 0 to 360 degree on concentric circles remains the same as the one of flat surface. If the shooting time of cloud imagery is known, through the imagery analysis or the analysis tools embedded in TSI-880, the sun's position on curved contours is not difficult to obtain; therefore, the curve fitting to build conversion polynomial (3) can be complete by means of finding the position of the sun in the flat and curved surface.

Suppose r_1 is the radial distance from the center to the pixel I in the curved image; r_s is the radial distance from the center to the pixel S in the corrected flat surface image; h is the vertical distance from the lens to the metal sphere base; and Θ the zenith, then

$$r_s = h \arctan\Theta \quad (1)$$

According to Marquez et al., who proposed correction algorithm that can analyze the changes in the relationship between the curved and the flat surface contours. Therefore, via the actual cloud statistical analysis, the relationship of r_1 with Θ is as follows:

$$r_1 = -0.1344\Theta^2 + 0.9024\Theta - 0.001799 \quad (2)$$

Since the corresponding zenith angle in the image coordinates and the sky coordinates is the same, the proportional ratio between r_s and r_1 can be calculated as k , $k = r_s / r_1$, set Φ is the polar angle of the pixel point (x_s, y_s), then

$$[x_s, y_s] = k r_1 [\cos\Phi, \sin\Phi] \quad (3)$$

According to the above formula, the corresponding relationship between pixels I and S can be obtained [4].

Image Interpolation Filling

After the distortion cloud image is recovered, near the center portion of the image almost remains the same because the pixels are combined when image shrinks, and the edge portion of the image is expanded causing pixels dispersed so that the existing pixels cannot fill the original space. Combined imaging display looks normal, where black dot image displayed in the expanded image, because the original pixel region is enlarged and there is no data to fill in, i.e., the RGB equal to zero in the enlarged area, shown as in Figure 5.

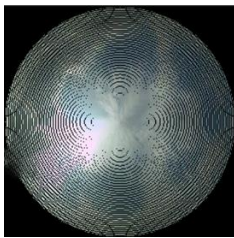


Fig 5. Black Dot in the Recovered Distortion Cloud Image

The simplest way to fill the vacancies of the expanded image is to take the average value of eight pixels surround each pixel, shown in Figure 6. If the pixel of the eight ones is vacant, it will be discarded in the calculation; vacant image after filled is shown in Figure 7.

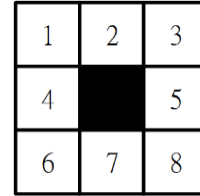


Fig. 6 Eight Pixels Surround Each Pixel



Fig. 7 Vacancies of the Expanded Image Filled

3. Sky Image Interpretation, Computation and Tracking

The nature of the visible light is a mixture of a certain ratio of the primary colors: red (R), green (G), blue (B), of which the center wavelength is 650 nm, 570 nm, 450 nm, respectively. A digital image contains the RGB luminance values, and to some extent it reflects the radiation intensity of the three bands. Therefore, the calculated ratio of red and blue of each pixel can tell whether it is cloud, and setting a reasonable threshold will determine what kind cloud is; this method is called threshold identification method.

Among all the present cloud recognition algorithms in the literature, there exists no paper to tell the cloud categories, e.g. cirrus, stratus, cumulus... However, different cloud optical thicknesses attenuate the solar radiation to a large extent. According to the translucent, clouds can be divided into the thin cloud and opaque cloud. While the thin cloud attenuates less solar radiation, the opaque cloud reduces greatly, or even blocks the solar radiation completely. Abide by the literature [5], different pixel ratios of red and blue can distinguish haze, opacity cloud and clear sky; accordingly, the radiation attenuation model can be established. First, the cloud pixel standardization (normalization), i.e., the red and blue ratio R needs to be defined.

$$R = \frac{b - r}{b + r} \quad (4)$$

where b and r represents the brightness value of blue and red channel, respectively.

Second, set the cloud segmentation threshold of the clear sky with thin cloud, and thin cloud with opaque cloud; i.e., η_{sky} and η_{thin} , in accordance with the following

formula determines the type of cloud pixels of

$$\begin{cases} \text{opaque cloud, } R \in [-1, \eta_{thin}) \\ \text{thin cloud, } R \in [\eta_{thin}, \eta_{sky}) \\ \text{clear sky, } R \in [\eta_{sky}, 1] \end{cases} \quad (5)$$

According to the literature [4], the statistics sample of η_{sky} and η_{thin} were 0.065 and 0.025. Based on these fixed thresholds, the outcome of the original sky and cloud image are drawn and shown, respectively, on the left, and the right side of Figure 8, where the blue area represents clear sky, gray area represents thin cloud, and the white area represents opaque cloud; the shooting time was 10:31 on September 16, 2015.

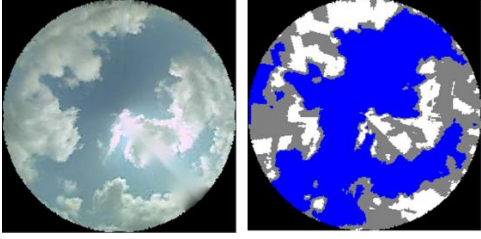


Fig. 8 Original Sky (left) vs. Cloud (right) Images

Cloudy Conditions

Under different weather conditions, the imaging character of the cloud is different, for example: cloudy sky image is significantly dimmer than the clear sky image. This is mainly because the cloud completely blocks the sun light in the cloudy day, causing the overall brightness of the image lusterless. Thus, if the fixed threshold method is employed to all the cases, the cloud computation will result in a bias error for the sake of the dim background.

According to the research analysis of Zhou Wen-jun et al.[6], the R (red) value in the image of the cloudy day is larger than the one of the sunny day, i.e., the B (blue) is relatively small; moreover, the saturated pixels in the cloudy image are less, which displays the sun is completely blocked by the cloud. Under the reign of standardization, the pixel ratio of red and blue if greater than 0.62 indicates that it is the thin cloud point, the pixel ratio between 0.3 and 0.62 is clear sky, where the opaque cloud point threshold is set at 0.66 (that is the pixel ratio between 0.66 and 1.0 is cloud point), while pixels from 0.62 to 0.66 may be thin cloud point, shown as the shaded area in the image, and it needs the further image analysis.

Making a comparison of the analysis result of Zhou's improved threshold method with the clear sky threshold by using the same image shut at 10:31 on September 16, 2015 as shown in Fig. 9. The result shows that the clear sky threshold overestimated the amount of the thin cloud, mistakenly deemed the opaque cloud as the thin cloud, and the total amount of cloud was miscalculated; nevertheless, the result of the improved threshold method reduces the amount of thin cloud, and

the opaque cloud amount and total cloud amount are closer to the actual observation results. It can be clearly seen that the improved threshold can effectively reduce the miscalculation of the thin cloud computing error, which is due to the different brightness background, and improve the accuracy of cloud calculation.

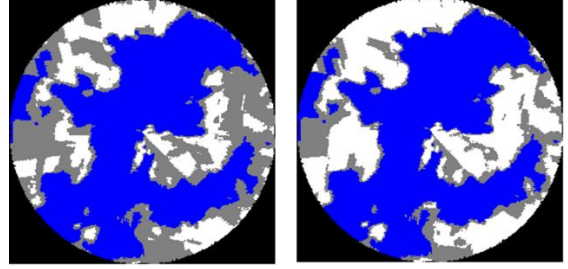


Fig. 9 Clear Sky Threshold (left) vs. Improved Threshold Method (right)

Cloud Tracking

With continuous cloud images of Total Sky Imager TSI-880, optical flow method [8] is used to detect the image pixel intensity changes over time, to make the pixel pairs with the least variable total strength, to infer cloud moving speed and direction. Lucas-Kanade method [9] and Horn Schunck method [10], i.e., equations (6)~(8) explain the benefits for less sensitivity to image noise and no need to compute the optical flow within the block under the condition of a smooth change in the entire image content.

$$\begin{bmatrix} V_x \\ V_y \end{bmatrix} = \begin{bmatrix} \sum_i I_x(q_i)^2 & \sum_i I_x(q_i)I_y(q_i) \\ \sum_i I_y(q_i)I_x(q_i) & \sum_i I_y(q_i)^2 \end{bmatrix}^{-1} \begin{bmatrix} -\sum_i I_x(q_i)I_t(q_i) \\ -\sum_i I_y(q_i)I_t(q_i) \end{bmatrix} \quad (6)$$

$$E = \iint [(Ixu + Iyv + It)^2 + \alpha^2 (\|\nabla u\|^2 + \|\nabla v\|^2)] dx \quad (7)$$

$$\begin{aligned} u^{k+1} &= \bar{u}^k - \frac{I_x(Ix\bar{u}^k + Iy\bar{v}^k + I_t)}{\alpha^2 + I_x^2 + I_y^2} \\ v^{k+1} &= \bar{v}^k - \frac{I_y(Ix\bar{u}^k + Iy\bar{v}^k + I_t)}{\alpha^2 + I_x^2 + I_y^2} \end{aligned} \quad (8)$$

By comparing different image processing skills such as the gray-scale transformation, red/blue ratio, YCrCb and the binary image processing technology, a better way to indicate the cloud motion is employed, shown as in the figures below. Also, the recent-first estimator method is utilized to evaluate and analyze the cloud motion and cloud cover factor to predict the solar energy, i.e., to estimate Global Horizontal Irradiance (GHI) and DNI. RFE is based on the recently observed behavior as the main basis, and takes the average value of the past behaviors as the estimation basis for the next behavior, which does not consider behavior pattern transforming.

$$v_{n+1} = \frac{\sum_i v_i}{n} \quad (9)$$

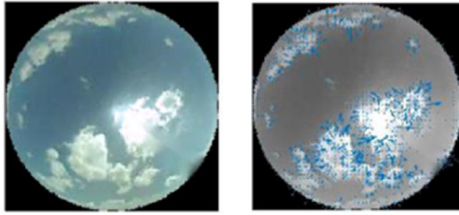


Fig. 10 Cloud Motion Tracking

4. Conclusion

In this study, the adopted enhanced algorithm has different thresholds set to distinguish the red-blue ratio of the pixels in order to more precisely tell the clear sky from the thin cloud, and the thin cloud from the thick cloud. Subsequently, the cloud pixel in the concentric circle is calculated. From the movement of the cloud vector, the short-term solar energy forecast (1 minute averaged GHI values for time horizons of <15 minutes ahead) is hence achieved. Of course, the short-term solar energy forecast will be more accurate as the values of classification algorithm and the size of concentric circle with the sun are carefully chosen. Moreover, if the wind direction and wind speed can be taken into consideration, the identification of cloud group reforming will be more practical and speeded up. The premise of making an accurate short-term solar energy prediction using the TSI-880 images lies in a precise cloud computation. In this paper, authors take the advantage of the digital processing technology to enhance the output images of TSI-880. In addition, the comparison of the clear sky threshold versus the improved fixed threshold has been made, and the way of promoting the accuracy of the cloud amount computation is discussed in detail. The theme of this study presented and explored is to research on and to improve in the cloud computing methods, which certainly becomes the first step of the solar energy prediction. For the further study on the GHI forecasting, there are two ways to proceed on the basis of this research: (1) taking the real-time calculated cloud amount and the historical data of the last few minutes as the input data for the estimation of the grey theory, which has been developed and technology transferred by INER; (2) to carry on the calculation and assessment of the cloud group movement by comparing two consecutive cloud images to estimate the centroid center. Then, detect the velocity of the cloud group vector, and make an evaluation to project the future cloud position, and finally utilize the cloud cover factor to predict the solar energy.

References

- [1] Yankee Environmental Systems, Inc. TSI-880 Automatic Total Sky Imager. Airport Industrial Park 101 Industrial Blvd. Turners Falls, MA 01376 USA);
- [2] Jiunn-Lin Wu, et al. "Using Image Inpainting to

Remove Dust Spots from Digital-SLR Images," Journal of Engineering National Chung Hsing Vol. 18, Issue 3, 2007;

[3] Ricardo Marquez, Carlos F. M. Coimbra, "Intra-hour DNI forecasting based on cloud tracking image analysis," Solar Energy 91 (2013) 327–336;

[4] Zhu Xiang, Zhou Hai, Ding Jie, Cheng Zhibao, and Ding Yuyu, "All-Sky Cloud Map Image Restoration Algorithm Research," Journal of Computer Aided Design & Computer Graphics, Vol. 26 No. 6 June 2014;

[5] Ding Yuyu, Ding Jie, Zhou Hai, Chen Zhibao, Cheng Xu, "Forecasting of Global Horizontal Irradiance in Photovoltaic Power Stations Based on the Total Sky Imager," Chinese Society for Electrical Engineering Vol. 1, No. 34;

[6] Zhou Wen-jun, Niu Sheng-jie, Xu Xiao-feng, 2014, "Improvements of Computational Methods for Cloud Cover Based on the Total Sky Imager," Transactions of Atmospheric Sciences 37(3): 289~296;

[7] S. Quesada-Ruiz, Y. Chu, J. Tovar-Pescador, H.T.C. Pedro, C.F.M. Coimbra, "Cloud-tracking methodology for intra-hour DNI forecasting," Solar Energy 102 (2014) 267–275.

[8] Berthold K.P. Horn and Brian G. Schunck, "Determining Optical Flow," Artificial Intelligence Laboratory, Massachusetts Institute of Technology, Cambridge, MA 02139, U.S.A.;

[9] Dhara Patel, Saurabh Upadhyay, "Optical Flow Measurement using Lucas Kanade Method," International Journal of Computer Applications (0975 – 8887), Volume 61– No.10, January 2013;

[10] Andres Bruhn, Joachim Weickert, Christoph Schnorr, "Lucas/Kanade Meets Horn/Schunck: Combining Local and Global Optic Flow Methods," International Journal of Computer Vision 61(3), 211–231, 2005

Acknowledgements

This work was supported and sponsored by the Nuclear Instrumentation Division of the Institute of Nuclear Energy Research (INER), Taiwan, and the image processing work as consignments were handed over to Dr. Raylan Huang of the Department of Information Engineering of I-Shou University, and Dr. Jin-Yinn Wang and Dr. Horng-Jyh Lin of Vanung University. Also, thanks Dr. Tsung-te, Lin, Mr. Cheng-dar Lee, Chih-po Kao and Miss Wan-li Hsu to provide the images of TSI-880 and the environmental weather data.